ACSNANO

www.acsnano.org

ARTICLE

Ultrasonic Steering Wheels: Turning Micromotors by Localized Acoustic Microstreaming

Qiang Gao, Zhou Yang, Ruitong Zhu, Jinping Wang, Pengzhao Xu, Jiayu Liu, Xiaowen Chen, Zuyao Yan, Yixin Peng, Yanping Wang, Hairong Zheng, Feiyan Cai, and Wei Wang*

Cite This: *ACS Nano* 2023, 17, 4729–4739

Read Online

ACCESS | Metrics & More | Article Recommendations | Supporting Information

ABSTRACT: **The ability to steer micromotors in specific directions and at precise speeds is highly desired for their use in complex environments. However, a generic steering strategy that can be applied to micromotors of all types and surface coatings is yet to be developed. Here, we report that ultrasound of ∼100 kHz can spin a spherical micromotor so that it turns left or right when moving forward, or that it moves in full circles. The direction and angular speeds of their spinning and the radii of circular trajectories are precisely tunable by varying ultrasound voltages and frequencies, as well as particle properties such as its radius, materials, and coating thickness. Such spinning is hypothesized to originate from the circular microstreaming flows localized around a solid microsphere vibrating in ultrasound. In addition to causing a micromotor to spin, such streaming flows also helped release cargos from a micromotor during a capture−transport−release mission. Localized microstreaming does not depend on or interference with a specific propulsion mechanism and can steer a wide variety of micromotors. This work suggests that ultrasound can be used to steer microrobots in complex, biologically relevant environments as well as to steer microorganisms and cells.**

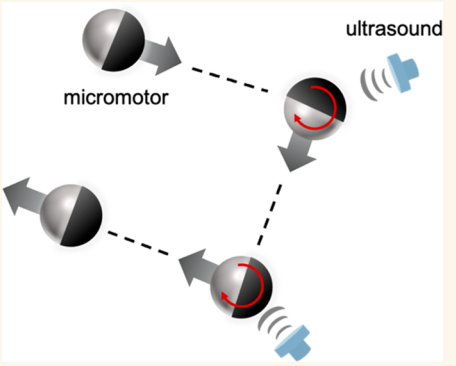

KEYWORDS: *micromotors, ultrasound, acoustic streaming, steering, universal, motion control*

Micromotors,[1−3] synthetic microparticles that autonomously move in liquids, are gaining attention because of their potential usefulness as microrobots in biomedical or environmental applications. In addition to efficient propulsion, these applications typically require a micromotor to steer through a complicated environment such as tortuous blood vessels or bifurcating microfluidic channels.[4−9] Steering is necessary even if a micromotor only needs to move in a straight line, which is complicated by Brownian motion, asymmetric particle shapes that arises from fabrication imperfections, or debris within the environments.

A micromotor can be steered by three common strategies. First, a magnetic micromotor can be steered by a magnetic field, generated by magnets or electromagnetic coils[10−14] or by placing a micromotor on a magnetic track.[15] Although effective and flexible, magnetic steering is only useful for magnetic samples. In addition, because all motors are magnetized and exposed to the same driving field, they are steered simultaneously and often in the same direction. Alternatively, a micromotor can find its way through taxis, i.e., migration along an external gradient.[16] Examples include chemotaxis in a chemical gradient,[17−19] rheotaxis in flows,[20−22] or phototaxis in a gradient of light intensities.[23] The disadvantage of taxis-based steering, however, is that it requires a long-range gradient and is less responsive. Finally, a micromotor can be guided by geometric confinements, such as walls, steps or grooves,[24−26] yet this strategy requires pre-established artificial microstructures. In light of these limitations, strategies that are generic, fast, easily accessible and tunable are highly desired for steering micromotors.

Given its biocompatibility and wide use in the clinics, ultrasound is an attractive candidate for powering and steering micromotors.[27,28] Previously, megahertz ultrasound has been demonstrated to power metallic microrods into fast axial propulsion and spinning in water.[27−30] Ultrasound of lower frequencies, in the range of tens to hundreds of kHz, have also

Received: November 6, 2022
Accepted: February 21, 2023
Published: February 23, 2023

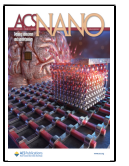

https://doi.org/10.1021/acsnano.2c11070
ACS Nano 2023, 17, 4729−4739

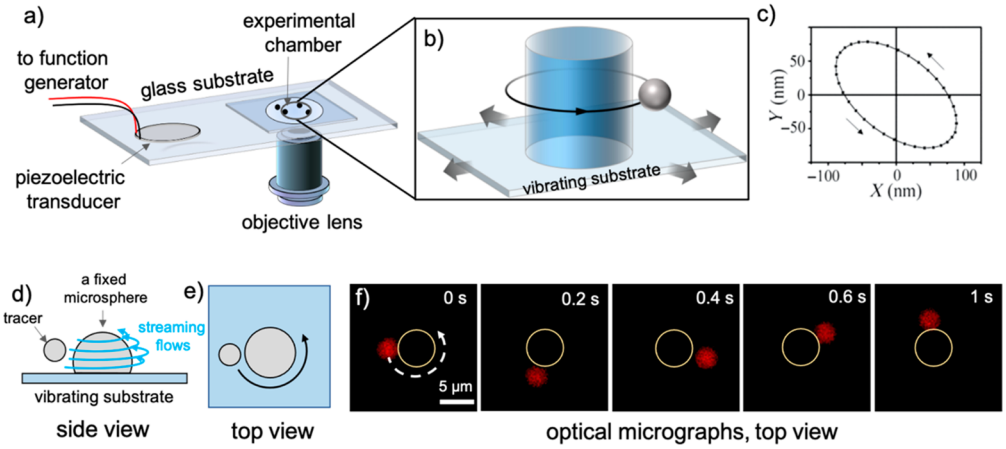

Figure 1. Localized acoustic microstreaming near a fixed micropillar. (a) Schematic of the experiment setup. See Figure S2 for an actual photo. (b) Advection of a tracer microsphere by the streaming flows circulating a fixed micropillar. The pillar and the substrate vibrate horizontally (shown in arrows) under the agitation of 100 kHz ultrasound. (c) Typical elliptical vibration of the substrate in the *x*–*y* plane measured by a laser Doppler scanning vibrometer, obtained from Figure 3a of ref 51. Reprinted in part with permission from ref 51. Copyright 2019 American Physical Society. (d) Side view and (e) top view of the circular motion of a tracer microsphere around a large polymer microsphere fixed onto a vibrating substrate. Blue and black curved arrows indicate the streaming flows and the advection of tracers, respectively. (f) Time-elapsed optical micrographs taken by confocal microscopy of a 3 μm PS microsphere (red fluorescence) orbiting at an angular speed of 4.3 rad/s around a fixed 5 μm PS sphere at the center (not fluorescent, circled in yellow), under ultrasound of 50 V and 110 kHz.

been used to power microcapsules via streaming flows from trapped air bubbles resonating in ultrasound.[12,31−36] Although ultrasound can turn a micromotor in these demonstrations, this is often achieved by either an asymmetric motor shape[37] or by an careful, asymmetric placement of resonating bubbles.[31,36] In neither case is ultrasound a generic, stand-alone steering tool, nor can it be applied to other types of micromotors.

We here report a generic ultrasonic steering strategy based on acoustic streaming,[38−40] which is a slip flow generated as acoustic waves travel across an interface between two pieces of materials of different acoustic properties. Our key discovery is that ultrasound generates a circular streaming flow localized around a microsphere sedimented above a substrate, and the sphere spins in the opposite direction to the flow. We also show that the rotational speed of such a spinning microsphere can be precisely controlled by varying the power and frequencies of the ultrasound, as well as the size, material compositions, and coating thickness of the sphere. Then, we demonstrate how this streaming-induced spinning can be used as a "steering wheel" to turn the direction of spherical micromotors powered by either electric fields or chemical reactions. Notably, acoustic steering bends motor trajectories into circles, the radii of which can be precisely tuned by varying the relative strength of the self-propulsion and the spinning of a motor. Finally, we show that localized streaming can be used to steer micromotors toward cargos and release them when needed.

Ultrasonic steering by localized acoustic streaming is fast, tunable, and applies to micromotors of different propulsion mechanisms, sizes, surface properties, and material compositions. Because torques are generated locally rather than imposed externally, each motor spins independently at their own directions and speeds. These are highly valuable features for steering micromachines in complex environments. The progress reported here is thus a major step toward using ultrasound for powering and controlling biomedical microbots.

RESULTS AND DISCUSSION

Spinning by Localized Microstreaming. It is long known that time-averaged, steady streaming flows are generated as acoustic waves pass through a medium, where the acoustic momentum flux is absorbed and energy is dissipated.[38−41] In particular, boundary-driven acoustic streaming flows arise as acoustic waves propagate across a solid−liquid interface.[42,43] These streaming flows can be localized as microstreaming,[44] especially near sharp edges[45,46] or oscillating bubbles.[47]

In the past few years, there have also been reports of localized microstreaming flows circulating a *micropillar* fixed on a vibrating substrate.[48−53] An example of such streaming flows is given in Figure 1. Here, a piezoelectric transducer is glued onto a piece of glass slide and next to a sealed, water-filled experimental chamber made of silicone. In this chamber were 5 μm polystyrene (PS) microspheres partially melted to the bottom glass slide ("micropillars", see Supporting Information for details of fixing) as well as 3 μm microspheres freely suspended as tracers. A previous measurement has shown that similar micropillars vibrated in elliptical trajectories in both *x* and *y* directions,[51] leading to circular microstreaming flows around the pillar. Indeed, we saw that 3 μm microspheres were advected in rough circles at 10.5 μm/s (4.3 rad/s) around the larger, fixed microspheres when agitated by ultrasound of 110 kHz and 50 V. Such circular microstreaming also occurs around nanopillars as small as 500 nm in diameter, as shown in Video S1. Note that ultrasound of driving frequencies of 100−200 kHz are used throughout this study, which yielded the strongest localized streaming. Lower or higher frequencies caused large-scale streaming flows that advected all microparticles, or no streaming at all beyond 1 MHz. At 100−200 kHz, our transducer is believed to vibrate in the radial mode, so that the substrate vibrated horizontally. More information is given in Figure S3.

Instead of a fixed micropillar, the surprising discovery was that a microsphere *unattached* to the bottom substrate (i.e., a

https://doi.org/10.1021/acsnano.2c11070
ACS Nano 2023, 17, 4729−4739

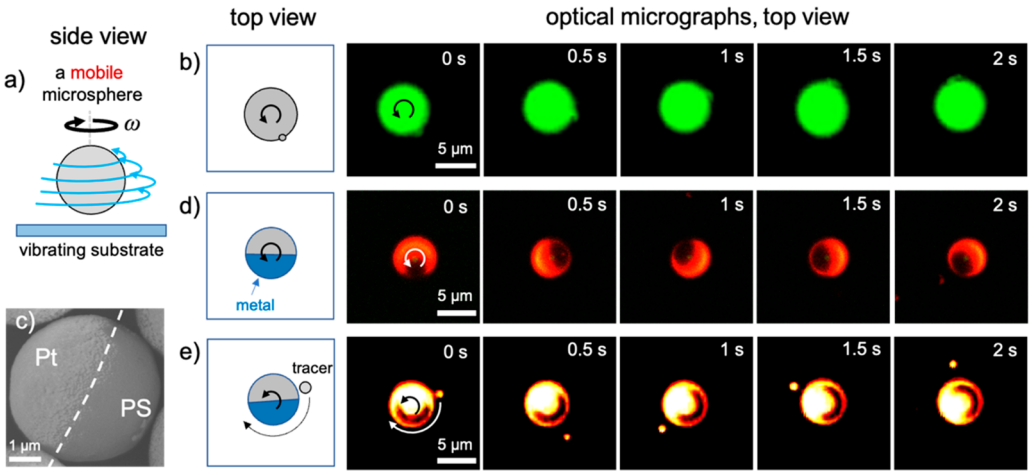

Figure 2. Mobile microspheres spin by localized acoustic microstreaming. (a) Schematic of a mobile microsphere spinning about an axis vertical to a vibrating substrate. Blue arrows represent streaming flows, and the black arrow indicates sphere spinning at an angular speed of ω. (b) Spinning of a fluorescent, isotropic 5 μm PS microsphere with a nanoparticle attached to its surface, taken from Video S1. (c) Scanning electron micrograph of a PS-Pt Janus microsphere. (d) In-place spinning of a PS-Pt Janus microsphere (the PS core is fluorescent and the Pt hemisphere is dark). (e) SiO_2-Pt Janus microsphere spins in the opposite direction to a nearby 1 μm PS microsphere, taken from Video S1. Ultrasound conditions: 75 V and 120 kHz in (b,d), 75 V and 113 kHz in (e).

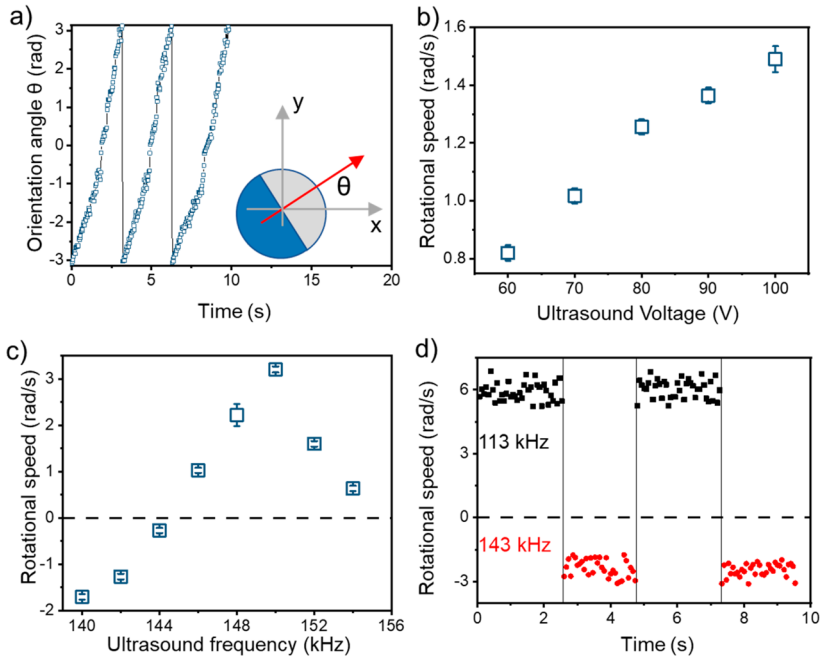

Figure 3. Tuning the spinning speed of a mobile microsphere by ultrasound parameters (data acquired from Video S10). (a) Change in the direction of a spinning PS-Pt Janus microsphere over time. The orientation angle θ is defined in the inset. (b,c) Time-averaged angular speed $\bar{\omega}$ of a spinning PS-Pt microsphere at different ultrasound voltages (b) and frequencies (c). Clockwise rotation is defined as positive. (d) Switching a PS-Pt microsphere between clockwise (black squares) and counterclockwise (red filled circles) spinning by switching between driving frequencies of 113 and 143 kHz, respectively. Error bars in (b,c) are standard errors from 10 microspheres during 5 s.

"mobile" microsphere) also generated steady, circular streaming flows around its body. More importantly, the sphere spun in place about an axis perpendicular to the substrate, in a direction opposite to the streaming flow (see Figure 2a for a cartoon illustration). As an example, Figure 2b and Video S1 show the steady spinning at 1.5 rad/s of a PS microsphere of 5 μm in diameter slightly above a glass substrate vibrating at 120 kHz. Here, the PS microsphere was *not* fixed to the substrate but was allowed to freely settle to the bottom substrate, which electrostatically repelled the sphere because both carried negative charges (-50.6 ± 0.2 and -68.1 ± 0.6 mV for the sphere and the substrate, respectively). The sphere then floated above the substrate and underwent typical Brownian motion in the absence of ultrasound.

Two additional examples further demonstrate the spinning of a mobile microsphere in ultrasound. In the first example, a positively charged (40.6 ± 0.5 mV) 500 nm fluorescent PS nanosphere was electrostatically attached to the surface of a negatively charged, 5 μm PS microsphere. We assumed that the presence of this nanosphere does not significantly affect the acoustic property or symmetry of the larger microsphere, supported by a previous study.[54] Acoustic spinning of the large

https://doi.org/10.1021/acsnano.2c11070
ACS Nano 2023, 17, 4729−4739

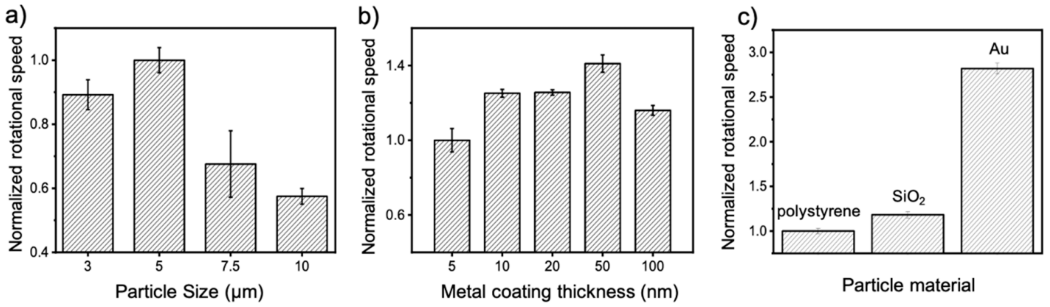

Figure 4. Spinning speeds of mobile microspheres of different types. (a−c) Normalized spinning speeds of microspheres of different diameters (a), coating thickness of Pt (b), or materials (c). SiO_2-Pt microspheres of 5 μm in diameters and half-coated with 10 nm of Pt were used in (a,b) except for cases where these parameters were varied. Isotropic PS and SiO_2 microspheres of 5 μm in diameters were used in (c), whereas solid Au microspheres of ∼4 μm in diameter were chemically synthesized and used in (c). Spinning speeds in (c) were determined by tracking tracers advecting in the vicinity of the particle under study. Error bars are standard errors from 10 microspheres during 5 s. Data are normalized to the value of 5 μm particles in (a), 5 nm metal coating in (b), and PS microspheres in (c).

sphere (with a nano-protrusion) can then be readily visualized in Figure 2b. Spinning is even more visible for a Janus microsphere. For example, Figure 2d,e and Video S1 show that a 5 μm PS microsphere half-coated with 10 nm of Pt (see Figure 2c for an electron micrograph) spun at 2.66 rad/s at 120 kHz ultrasound. Such Janus microspheres are used for the rest of the article for studying streaming-induced spinning, because their rotation was easier to identify and quantify than isotropic microspheres, even though both spin in qualitatively the same way in ultrasound.

Such acoustic spinning of mobile microspheres is a robust observation: it was observed for microspheres made of polymers, SiO_2, and metal (see Figure 4c and Figure S4), microspheres of a wide range of sizes (Figure 4a) and coated with metal of different thickness (Figure 4b), in experimental chambers of diameters ranging from 1 to a dozen mm, in chambers shaped in triangles, circles, squares, or even in the absence of any chamber (i.e., in a water droplet), and on substrates made of glass or silicon wafers (the results of the experiments performed in different chambers and substrates are not shown). Preliminary experiments also confirmed that a snowman-shaped colloidal dimer could also spin, which stands with its long axis vertical to the substrate and spins around this axis (see Video S9).

We do not fully understand why a mobile microsphere spontaneously spin in ∼100−200 kHz ultrasound, but we speculate that it is caused by the same circular, localized acoustic streaming that occurs near fixed micropillars. A tentative mechanism is given below, and the key is the observation that a mobile microsphere spins in the opposite direction to its surrounding fluid. For example, Figure 2e shows a 1 μm polymer tracer sphere being advected into orbiting a spinning 5 μm SiO_2-Pt Janus microsphere. Here, the tracer moved clockwise, while the center Janus sphere spun counterclockwise. The circular acoustic streaming flows around a Janus microsphere are suspected to arise from the same physical reasons as those around a fixed pillar:[48−53] as sound waves propagate across the solid−water interface, momentum is transferred from a vibrating sphere to the fluid, imparting torques that leads to vortices. Following the Newton's third law, the sphere (fixed to the substrate or not) reciprocally and simultaneously receives a torque from the fluid. Importantly, this torque does nothing to a *fixed* microsphere that is held in place, but spins a *mobile* microsphere that is free to rotate, so that it spins opposite to the surrounding flows to conserve angular momentum of the entire system. This tentative mechanism will be followed by a later study with more quantitative and rigorous understanding.

Tuning the Spinning. Before using localized acoustic streaming to turn a micromotor, we first show that the direction and speed of a spinning microsphere can be precisely tuned by varying a number of experimental parameters. First, we quantified the angular speed ω of a spinning microsphere from the temporal variation of its direction θ (see Figure 3a for definition), so that its average angular speed $\bar{\omega} = \langle d\theta/dt \rangle_t$, where $\langle \rangle_t$ refers to taking the time average. We then examined $\bar{\omega}$ as a function of the ultrasound voltages (V) and driving frequencies (f), as well as the size (sphere diameter), material composition, and coating thickness of the microsphere. Results in Figure 3b show that, intuitively, a microsphere spins faster at higher ultrasound voltages that inject more energy into the system, in agreement with previous studies on circular acoustic streaming flows around fixed micropillars.[48,51−53]

Less intuitively, Figure 3c shows that a microsphere could reverse its spinning direction as the driving frequencies changed. Over a larger frequency range, such direction switching can occur multiple times, shown in Figure S5 and Video S11. Similar direction reversal of streaming flows around micropillars upon changing driving frequencies has been reported in the literature[48,53] and was attributed to a change in the vibrational mode of the substrate. Such direction switching is highly reproducible, as shown in Figure 3d, where the clockwise and counterclockwise spinning of a 5 μm PS microsphere is switched back and forth by switching the driving frequencies between 113 and 143 kHz.

The spinning speeds of a microsphere are also related to their intrinsic properties such as sizes, materials or coating thickness. For example, Figure 4a shows that larger microspheres spun more slowly than smaller spheres made of the same material and activated under the same ultrasound. However, acoustic spinning was *not* observed for mobile Janus PS-Pt nanospheres of 500 nm diameter, or gold nanorods of 3 μm long and 300 nm in diameter. We suspect a few physical effects could collectively determine how sizes affect the spinning speeds: a larger particle could experience a stronger streaming flow but is counteracted by larger viscous drags that not only scales with $6\pi\eta a$ (a being particle radius) but also increases as a larger particle gets closer to the bottom. Increasing the thickness of the metal coating of a metal−polymer Janus microsphere from 5 to 50 nm increased the

https://doi.org/10.1021/acsnano.2c11070
ACS Nano 2023, 17, 4729−4739

spinning speeds by ~40% (Figure 4b), but an even thicker coating caused slower spinning, possibly because of an increase in particle size.

Materials play a major role in determining the spinning speed of a mobile microsphere. For example, Figure 4c shows that SiO_2 microspheres spin faster than polymer spheres, and Au microspheres were even faster. This difference could be related to the different acoustic contrast factors of PS (0.22), SiO_2 (0.59), and Au (0.79) (see Supporting Information for definitions and calculations), which causes microspheres made of different materials to vibrate and stream in different magnitudes. However, the ratio of their spinning rates does not exactly match that of their acoustic contrast factors. Figure S4 further shows that AuPt Janus microspheres spin significantly faster than either PS-Pt or SiO_2-Pt Janus spheres, in qualitative agreement with the above discussion. The choice of the metal for the cap material (Au vs Pt), however, had a minor effect on the spinning speed of a Janus microsphere (Video S10).

Although a detailed understanding of how various parameters affect the spinning speeds of a microsphere is lacking at this moment, it is clear that ultrasonic spinning of mobile microspheres is widely found in a variety of samples and under different operating conditions. More importantly for applications, these results show that the direction and magnitude of a spinning microsphere can be tuned.

Ultrasonic Steering of Micromotors. The acoustic spinning of microspheres described above can be used to steer micromotors that tend to move in tortuous, diffusive trajectories.[55,56] The idea is simple: ultrasound is applied every time a micromotor needs to make a turn, so that the motor is steered to a direction and with an angle precisely determined by humans operators. In Figure 5, we demonstrate the usefulness and generatability of ultrasonic steering with two types of micromotors. In each case, a spherical micromotor self-propels slightly above a glass substrate, and ultrasound is turned on and off via a ceramic transducer located next to the experimental chamber as in the case of Figure 1. Both types of micromotors are made of PS-Pt Janus microspheres but powered differently. The first type (Figure 5a–c and Video S2) moves in an alternating current (AC) electric field by asymmetric electroosmotic flows, a mechanism known as induced charge electrophoresis (ICEP).[57−60] The second type (Figure 5d–f and Video S3) catalyzes the decomposition of H_2O_2 into O_2 and water on the Pt cap, and the resulting chemical gradient powers the motor via self-phoresis.[55,56,61−63] A third example of the ultrasonic steering of a photochemically powered TiO_2-Pt micromotor is given in Video S4. It showed qualitatively the same result as a SiO_2-Pt motor, and not elaborated here.

The precision of ultrasonic steering is perhaps better illustrated with the electrical micromotors shown in Figure 5a–c, given their relatively straight trajectories. Importantly, although all micromotors were steered simultaneously when ultrasound was applied, they moved in independent trajectories (Figure 5c and Video S5). This is in stark contrast to magnetically steered micromotors whose trajectories are strongly correlated (see Figure S11 in ref 64). This difference, elaborated below, is fundamentally rooted in how steering is achieved in either case: magnetic steering works by aligning a magnetic micromotor with an external magnetic field, while ultrasonic steering works by an individual micromotor generating its own torque locally.

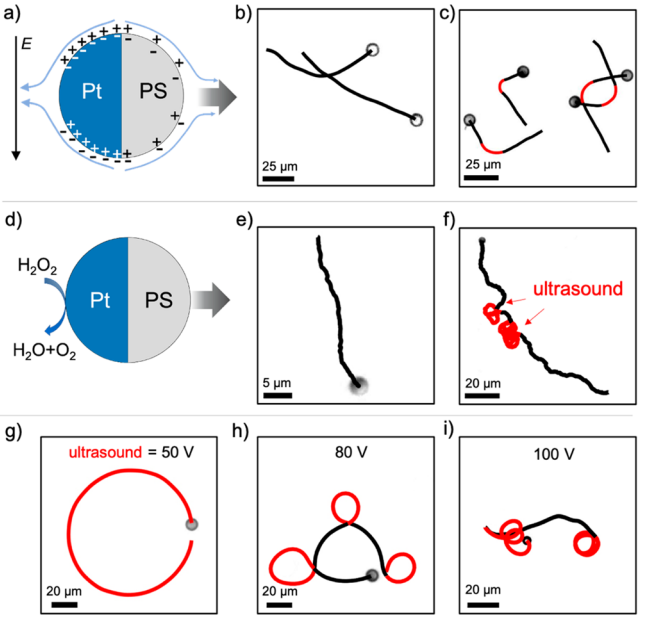

Figure 5. Ultrasonic steering of electrically (a–c) and chemically (d–f) powered micromotors. The sections of trajectories under ultrasonic steering are marked red. (a,d) Schematics of the propulsion mechanisms of micromotors powered by alternating current (AC) electric fields (a) and surface catalysis of H_2O_2 (d). See main text for details. (b–f) Typical trajectories without (b,e) and with (c,f) ultrasonic steering. (g–i) Circular trajectories of different radii of electrically powered micromotors steered by ultrasound of different voltages (marked in red). Experimental conditions: AC electric field of 400 V/cm and 1 kHz for (b,c) and (g–i); ultrasound of 75 V and 110 kHz for (c,f); 3% H_2O_2 for (e,f); ultrasound of 183, 120, and 153 kHz for (g–i), respectively. Videos S2, S3, and S6 correspond to (b,c), (e,f), and (g–i), respectively.

While a short burse of ultrasound turns a motor left or right, prolonged ultrasound turns a micromotor in circles. Importantly, the radius R of the circular trajectory can be fine-tuned following $R = U/\omega$, where U is the motor's intrinsic self-propulsion speed and ω is the angular speed caused by acoustic spinning. Both U and ω are easily tunable, yet decoupled from each other. For example, in the case of an electrical micromotor, U varies with the driving amplitude and/or frequency of the AC electric field, while ω varies with those of ultrasound. By adjusting the relative magnitude of U and ω, a micromotor can be steered into circular trajectories of different R. For example, Figure 5g–i and Video S6 showcase electrical micromotors moving in circular trajectories of three different R: large orbits of R = 23.9 μm (Figure 5g, U = 16.1 μm/s and ω = 0.67 rad/s), medium sized circles of R = 11.5 μm (Figure 5h, U = 24.8 μm/s and ω = 2.16 rad/s), and tight circles of R = 5.7 μm (Figure 5i, U = 13.9 μm/s and ω = 2.44 rad/s). The trajectories of a chemical micromotor can, in principle, be tuned, as well, for which U is typically a function of fuel concentration (experiments not performed).

Acoustic Spinning in a Capture–Transport–Release Mission. Taking ultrasonic steering one step further toward an application, we demonstrate in Figure 6 and Video S7 a crude example of its usefulness in microscopic cargo transport. Here, ultrasound not only steers a micromotor toward specific cargos, but also releases cargoes when needed. The operating principle is illustrated in Figure 6a. As an example, Figure 6b

https://doi.org/10.1021/acsnano.2c11070
ACS Nano 2023, 17, 4729–4739

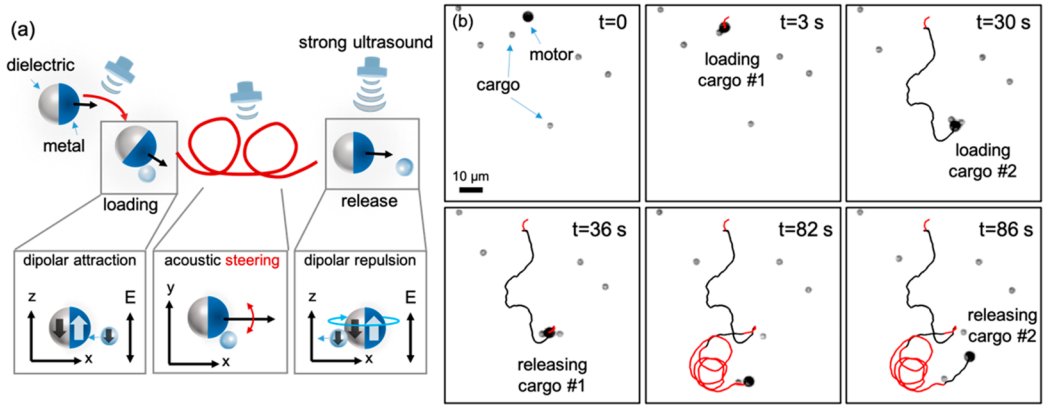

Figure 6. Cargo pickup, transport, and release enabled by acoustic spinning. (a) Schematic of the operation. The motor is a metal dielectric Janus microsphere moving in AC electric fields. Inset, left: at high AC frequencies (e.g., 1 MHz), the Janus microsphere moves toward the metal cap and attracts polymer tracers to the metal cap by dipolar attractions.[65,66] Inset, middle: ultrasound is used to steer the micromotor, and its trajectory under ultrasonic steering is marked red. Inset, right: when in need of releasing the captured cargo, a strong pulse of ultrasound is applied that causes strong streaming flows around the motor, which brings the cargo close to the dielectric hemisphere and releases it by dipolar repulsion. The motor−tracer conjugate can be steered into arbitrary trajectories before the cargo is released. (b) Series of optical micrographs demonstrating one example of (a). Here, a 5 μm SiO_2-Pt Janus microsphere moved in an AC electric field of 1 MHz and 250 V/cm in water. It picked up two 2 μm SiO_2 microspheres as it moved. Ultrasound of 113 kHz and 50 V was used to steer the motor, and ultrasound pulses of 113 kHz and 100 V were turned on for 1 s at t = 36 and t = 82 s to release two cargos. The two spheres were not released together likely because of the randomness of their initial positions when ultrasound was applied. See the Supporting Information for experimental details.

shows a 5 μm Pt-SiO_2 Janus micromotor, powered by 1 MHz AC electric fields, picked up two 2 μm SiO_2 tracers (as cargos) sequentially by dipolar interactions (principles of attraction are detailed in refs 65 and 66 and described in Figure S6). Ultrasound was turned on very briefly at the beginning to turn the motor toward cargo #1 rather than other cargos scattered around. The motor−tracer conjugate then moved on its own course and picked up cargo #2 by the same dipolar attraction that captured #1. Later, cargos were released by a short, powerful ultrasound pulse of 100 V. This was much stronger than that used for steering (50 V), thus generating strong streaming flows that spun the cargo around the motor to the SiO_2 side. The cargo is then released by dipolar repulsion because both the cargo and the SiO_2 hemisphere are electrically polarized in the same direction. The second cargo was later released by the same mechanism, after the motor was acoustically steered for some time. The operations described above, "steered capture"−"steered transport"−"release", could, in principle, be optimized and fully automated to enable applications such as microrobotic cell manipulations in a microfluidic chip.

Differences between Ultrasonic and Electromagnetic Steering. The ultrasonic steering strategy we proposed and demonstrated here is fundamentally different from other strategies that turn micromotors by external torques, such as magnetic spheres in rotating magnetic fields[67] or Ni nanowires in rotating electric fields.[68] This difference might not be obvious, given that in both cases energy is applied from an external source to the entire population, and in both cases all particles spin simultaneously. However, ultrasound breaks *local*, rather than *global*, symmetry. As a result, a microsphere spins *by itself*, with a frequency and a spinning direction controlled but not dictated by acoustic parameters. Electromagnetic spinners, on contrary, rotate in the same direction as the field, and with the same frequency as the field (unless the field frequency is too high for it to catch up).[69]

These fundamental differences between electromagnetic and acoustic spinning lead to two distinct modes of trajectories, shown as oversimplified cartoons in Figure 7. In terms of

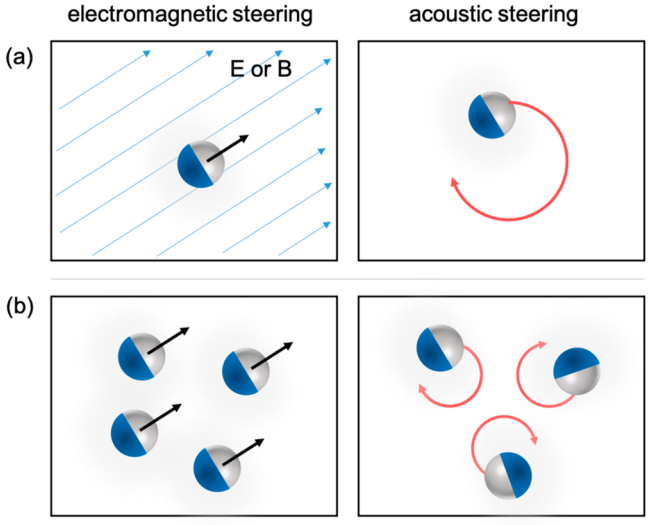

Figure 7. Differences between electromagnetic (left) and acoustic (right) steering. (a) Motors align with the field lines if steered by an electromagnetic field (left) but rotate in circles if steered by ultrasound (right). (b) Population of motors move in the same direction if steered by an electromagnetic field (left) but move in independent trajectories if steered by ultrasound (right). These cartoons are schematics and oversimplified.

trajectory shapes (Figure 7a), electromagnetically steered motors move in straight trajectories parallel or perpendicular to the external field lines, while ultrasound steers motors into circles. This distinction could also lead to different hydrodynamic interactions among colloidal particles spun by electromagnetic fields or acoustic streaming, a topic to be

https://doi.org/10.1021/acsnano.2c11070
ACS Nano 2023, 17, 4729−4739

explored in a separate study. In terms of directionality (Figure 7b), a population of electromagnetically steered motors all move in the same direction (or two orthogonal directions depending on their magnetization).[11] Acoustically steered motors, on the other hand, move in their own directions, but all turning by the same angle (ideally) dictated by the acoustic spinning.

Neither of these two steering strategies, ultrasonic or electromagnetic, is necessarily "better" than the other, but they could be better suited for a specific task or application. For example, electromagnetic steering could be more useful if all motors are expected to move toward the same target, while ultrasonic steering could be more useful if autonomy is needed or the motors are expected to probe their local environment. We also note that the principle of acoustic steering is similar to the run-and-tumble strategy proposed in ref 57, where electrically powered micromotors switch between moving linearly or in circles when the electric frequencies are switched. The key advantage of our ultrasonic steering strategy, however, is that it is independent of the motor's propulsion, thus applicable to a much wider variety of micromotors than ref 56.

Applicability of Ultrasonic Steering. Acoustic spinning and its related use in ultrasonic steering is a robust, highly reproducible and generic physical effect, as long as the experimental condition permits localized, circular acoustic microstreaming. As a result, we observed spontaneous spinning of microspheres of different sizes, shapes, and compositions in experiments performed under a range of acoustic parameters and in different experimental chambers and on different substrates. Moreover, we have demonstrated successful acoustic steering with micromotors of three different types (one powered by electric fields, and two by chemical reactions). These results strongly suggest that acoustic spinning is a generic and versatile technique to spin microscopic objects in a contactless and controllable manner. Furthermore, given the rich literature of using acoustic streaming to manipulate cells and microorganisms,[49,70−72] we are optimistic that acoustic spinning reported here can be used to spin microorganisms or cells that are not stuck on a substrate.

Limitations of Ultrasonic Steering. The ultrasonic steering of a micromotor can be improved in a few aspects. Perhaps the biggest limitation is that all motors in a population are simultaneously steered because ultrasound is applied globally, rather than individual steering that is sometimes desired. Note that this statement is not contradicting the features described in the section Differences between Ultrasonic and Electromagnetic Steering because even though all motors are steered by ultrasound *simultaneously*, they do not move in the same direction as in the case of electromagnetic steering. Nevertheless, to make each motor individually addressable, one could make each motor slightly different, so that they only respond to a specific set of acoustic parameters. A similar strategy has been applied to magnetic micromotors to make each motor individually addressable.[36,73−77]

A second limitation is that not all microspheres in the field of view spin the same way: some spin fast, while others might spin more slowly, do not spin, or even spin in the opposite direction (see examples in Videos S8 and S11). This variance of spinning states could be because microspheres of slightly different diameters and coatings were used. However, it is more likely due to the nonuniformity of the acoustic field: different points on the substrate could vibrate in different phases or amplitudes, depending on the vibrational modes of the entire system at a specific frequency. The distribution of the acoustic energy is also affected by the exact location of the piezoelectric transducer, and by the sound scattering off the chamber walls. As a result, it is challenging to precisely steer a micromotor that moves across the substrate, because the acoustic frequency required to turn it toward a specific direction and at a specific rate varies from one spot to another. This issue could be solved by more careful designs of the experimental setup and the use of a pair of transducers with well-defined phase differences, as in ref 49, so that the exact distribution of acoustic fields is known.

Finally, although not discussed in this article, global forces such as acoustic radiation forces[78] and the drag force induced by global streaming flows,[79] which are concurrent effect with localized microstreaming discussed here, could transport or even collect micromotors,[80] and thus obstruct their steering (see Video S11 for an example). Because these effects are sensitive on the driving frequencies and locations on the substrates, a micromotor could move in unintended directions when the acoustic frequency is changed, or when the motor moves to a different spot. This issue of uncontrolled transport can be mitigated, or even taken advantage of, by careful experimental designs that produces well-established acoustic fields of known distributions. Global streaming could also be mitigated by the use of pulsed ultrasound.[81]

CONCLUSIONS

In summary, we have reported a generic strategy to steer micromotors with ultrasound, taking advantage of the self-spinning of a microsphere in ultrasound of ∼100−200 kHz. Such spinning is tentatively attributed to localized, circular streaming flows, but a complete mechanistic understanding is lacking. The spinning speed and direction of a microsphere can be precisely controlled by the driving voltage or frequencies of the ultrasound, or by the size, material, and coating thickness of the particle. Such acoustic spinning was then used to steer two types of micromotors, one powered by surface catalysis, the other by AC electric field. By tuning the ratio of the motor's self-propulsion speed with its spinning speed, a motor can be steered to move in trajectories of different tightness. Using acoustic spinning, we have also demonstrated a crude example of how a micromotor can approach and pick up cargos, release them on demand, and transport cargos along steered trajectories.

Acoustic spinning and its use in steering micromotors is a fundamentally different strategy from electromagnetic steering, in both the directionalities of the motors, and the shapes of the resulting trajectories. This difference is derived from the fact that acoustic spinning breaks *local* chiral symmetry, so that each particle spins by itself. Moreover, acoustic spinning works for motors of different propulsion mechanisms, a major advantage in the controlled operation of microrobots in complex environment, particularly those powered and steered by biocompatible ultrasound. Furthermore, acoustic spinning works for particles of a variety of sizes and compositions, so that it could be developed into a generic and versatile tool for rotating microscopic objects contactlessly and controllably, including living microorganisms and cells.

METHODS

Sample Synthesis. Polystyrene (PS) and SiO_2 microspheres of various sizes were purchased from Tianjin Baseline Chrometch

https://doi.org/10.1021/acsnano.2c11070
ACS Nano 2023, 17, 4729−4739

Research Center. Janus microspheres were fabricated by sputter-coating on a monolayer of microspheres with Pt of typically 5−10 nm. The choice of the sputtered metal, or whether it is sputter-coated or thermally evaporated, is not important. Gold microspheres were chemically synthesized following ref 82, and spheres of different size ranges were separated by centrifugation. TiO_2 microspheres were chemically synthesized following ref 83 by coating commercial SiO_2 microspheres with a thin TiO_2 shell. Scanning electron micrographs of gold and TiO_2 microspheres are given in Figure S1.

Snowman-shaped colloidal dimer were synthesized following ref 84. In a typical experiment, 20 mg of TiO_2 particles was dissolved in 30 mL of deionized water (DI) and sonicated for 15 min. Then, 100 μL of $NH_3{\cdot}H_2O$ was added, followed by the addition of 300 μL of 3-(trimethoxysilyl)propyl methacrylate (TPM) monomer, and the mixture was kept under stirring for 1 h. To dewet the TPM from the TiO_2 particles, a desired amount of Triton X-100 (TX) was added to the mixture. The extent of dewetting can be controlled by varying the concentration of TX (C_{TX}). Then the polymerization of the TPM oil was realized by adding 10 mg of AIBN and heating the solution at 80 °C for 6 h. The resulting particles were cleaned by multiple cycles of sedimentation and resuspension in deionized water. Optical micrograph of snowman-shaped colloidal dimers are given in Figure S1.

The zeta-potential of the glass substrate was measured by Zetasizer ZEN1020, Malvern, in deionized water. The zeta-potential of microspheres was measured by Zetasizer Nano ZSP, Malvern, in deionized water. Each measurement was performed automatically for 12−15 cycles and repeated for 3 times.

Experimental Setup. A piezoelectric ceramic transducer (model SMD12T06R412WL, STEMINC) was glued by epoxy to the conductive side of an indium tin oxide glass slide (70 mm × 25 mm). The ceramic disk was 0.6 mm thick and 12 mm in diameter and had a nominal resonating frequency of 3.4 MHz. Next to the transducer and on the same side of the ITO slide, attached a silicone spacer of 200 μm thick with a circular hole of 6 mm in diameter. Colloidal suspension was pipetted into the hole, and a clean coverslip was placed on the top to seal the chamber. Care was needed to prevent air bubbles from being trapped in the chamber. A cartoon schematic of the experimental setup is given in Figure 1a in the main text, and an actual photo is shown in Figure S2.

To fix PS microspheres onto a substrate, their aqueous suspension was drop-casted on a piece of glass slide. After drying, the slide was placed on a hot plate and heated at 90 °C for 20 s, so that PS spheres partially melted and stuck on the slide surface to serve as fixed micropillars.

Micromotor Experiments. ITO slides were used as both the top and the bottom substrates for experiments with electrically powered micromotors shown in Figure 5a−c and Figure 6. These two electrodes were connected to a function generator via conductive copper tapes, and sine waves of typically 8 V were applied. The driving frequencies were typically 1 kHz for experiments in Figure 5a−c and 1 MHz for Figure 6. A schematic of the experimental setup is shown in Figure S3. Chemically powered SiO_2-Pt micromotors moved in 3% H_2O_2. Photochemically powered TiO_2-Pt micromotors moved in 2% H_2O_2 under UV light of 365 nm (model M365LP-C1, Thorlabs) at a power density of 60.3 mW/cm^2.

Microscopic Imaging and Tracking. In a typical experiment, an inverted optical microscope (model IX73, Olympus) was used to observe samples from below (videos recorded at 15 fps with a CMOS camera). Occasionally, confocal microscopy (SP8, Leica) was used to record fluorescent videos of high spatial resolutions (at 4 fps, such as Figure 2d). To calculate the rotational speed of a spinning microsphere, its orientation angle θ (see Figure 3a for definition) was identified with a homemade MATLAB code, by first identifying the circular contour with Circle Finder APP, then drawing an arrow that points from the black to the white hemispheres. Trajectories of a micromotor were obtained by tracking the particle with homemade MATLAB codes, courtesy of Prof. Hepeng Zhang from Shanghai Jiaotong University.

ASSOCIATED CONTENT

Supporting Information

The Supporting Information is available free of charge at https://pubs.acs.org/doi/10.1021/acsnano.2c11070.

Video S1: Circular streaming flows (MP4)

Video S2: An electrically powered micromotor steered by ultrasound (MP4)

Video S3: A chemically powered micromotor steered by ultrasound (MP4)

Video S4: A light-powered micromotor steered by ultrasound (MP4)

Video S5: Individual steering of several micromotors (MP4)

Video S6: Tuning the trajectories of micromotors by adjusting ultrasound voltages (MP4)

Video S7: Microscopic cargo transport (MP4)

Video S8: Microspheres spinning differently (MP4)

Video S9: Acoustic spinning of a snowman-shaped colloidal dimer (MP4)

Video S10: Spinning of microspheres at different ultrasound voltages and frequencies, and made of Au or Pt caps (MP4)

Video S11: Spinning of multiple microspheres in a field view across a wide range of ultrasound frequencies (MP4)

Sample synthesis (Figure S1), experimental setup (Figure S2), micromotor experiments (Figure S6), details on calculations of acoustic contrast factors (Table S1), and ultrasound measurement (Figures S3−S5) (PDF)

AUTHOR INFORMATION

Corresponding Author

Wei Wang − *Sauvage Laboratory for Smart Materials, School of Materials Science and Engineering, Harbin Institute of Technology (Shenzhen), Shenzhen 518055 Guangdong, China*; Email: weiwangsz@hit.edu.cn

Authors

Qiang Gao − *Sauvage Laboratory for Smart Materials, School of Materials Science and Engineering, Harbin Institute of Technology (Shenzhen), Shenzhen 518055 Guangdong, China*

Zhou Yang − *Sauvage Laboratory for Smart Materials, School of Materials Science and Engineering, Harbin Institute of Technology (Shenzhen), Shenzhen 518055 Guangdong, China*

Ruitong Zhu − *Sauvage Laboratory for Smart Materials, School of Materials Science and Engineering, Harbin Institute of Technology (Shenzhen), Shenzhen 518055 Guangdong, China*

Jinping Wang − *Paul C. Lauterbur Research Centre for Biomedical Imaging, Shenzhen Institutes of Advanced Technology, Chinese Academy of Sciences, Shenzhen 518055 Guangdong, China*

Pengzhao Xu − *Sauvage Laboratory for Smart Materials, School of Materials Science and Engineering, Harbin Institute of Technology (Shenzhen), Shenzhen 518055 Guangdong, China*

Jiayu Liu − *Sauvage Laboratory for Smart Materials, School of Materials Science and Engineering, Harbin Institute of*

https://doi.org/10.1021/acsnano.2c11070
ACS Nano 2023, 17, 4729−4739

Technology (Shenzhen), Shenzhen 518055 Guangdong, China

Xiaowen Chen − *Sauvage Laboratory for Smart Materials, School of Materials Science and Engineering, Harbin Institute of Technology (Shenzhen), Shenzhen 518055 Guangdong, China*

Zuyao Yan − *Sauvage Laboratory for Smart Materials, School of Materials Science and Engineering, Harbin Institute of Technology (Shenzhen), Shenzhen 518055 Guangdong, China*

Yixin Peng − *Sauvage Laboratory for Smart Materials, School of Materials Science and Engineering, Harbin Institute of Technology (Shenzhen), Shenzhen 518055 Guangdong, China*

Yanping Wang − *Paul C. Lauterbur Research Centre for Biomedical Imaging, Shenzhen Institutes of Advanced Technology, Chinese Academy of Sciences, Shenzhen 518055 Guangdong, China*

Hairong Zheng − *Paul C. Lauterbur Research Centre for Biomedical Imaging, Shenzhen Institutes of Advanced Technology, Chinese Academy of Sciences, Shenzhen 518055 Guangdong, China;* orcid.org/0000-0002-8558-5102

Feiyan Cai − *Paul C. Lauterbur Research Centre for Biomedical Imaging, Shenzhen Institutes of Advanced Technology, Chinese Academy of Sciences, Shenzhen 518055 Guangdong, China*

Complete contact information is available at: https://pubs.acs.org/10.1021/acsnano.2c11070

Notes

The authors declare no competing financial interest.

ACKNOWLEDGMENTS

The study carried out at HIT (Shenzhen) has been financially supported the Shenzhen Science and Technology Program (RCYX20210609103122038, JCYJ20190806144807401, JCYJ20210324121408022), and by the National Natural Science Foundation of China (11774075). Hairong Zheng, Jinping Wang, and Feiyan Cai are financially supported by the National Natural Science Foundation of China (11974372 and 12004409). We are grateful for the helpful discussions with Prof. Xu Zheng at the Institute of Mechanics, CAS, and for Ms. Ting Kuang at the Education Center of Experiments and Innovations at HIT (Shenzhen) for her assistance with confocal microscopy.

REFERENCES

(1) Chen, X.; Zhou, C.; Wang, W. Colloidal Motors 101: A Beginner's Guide to Colloidal Motor Research. *Chem.—Asian J.* **2019**, *14* (14), 2388−2405.

(2) Credi, A. Nanomachines. Fundamentals and Applications. By Joseph Wang. *Angew. Chem., Int. Ed.* **2014**, *53* (17), 4274−4275.

(3) Mallouk, T. E.; Sen, A. Powering Nanorobots. *Sci. Am.* **2009**, *300* (5), 72−77.

(4) Rao, K. J.; Li, F.; Meng, L.; Zheng, H.; Cai, F.; Wang, W. A Force to Be Reckoned With: A Review of Synthetic Microswimmers Powered by Ultrasound. *Small* **2015**, *11* (24), 2836−2846.

(5) Teo, W. Z.; Pumera, M. Motion Control of Micro-/Nanomotors. *Chem.—Eur. J.* **2016**, *22* (42), 14796−14804.

(6) Yang, Q.; Xu, L.; Zhong, W.; Yan, Q.; Gao, Y.; Hong, W.; She, Y.; Yang, G. Recent Advances in Motion Control of Micro/Nanomotors. *Advanced Intelligent Systems* **2020**, *2* (8), 2000049.

(7) Yu, S.; Cai, Y.; Wu, Z.; He, Q. Recent Progress on Motion Control of Swimming Micro/Nanorobots. *VIEW* **2021**, *2* (5), 20200113.

(8) Jiang, J.; Yang, Z.; Ferreira, A.; Zhang, L. Control and Autonomy of Microrobots: Recent Progress and Perspective. *Advanced Intelligent Systems* **2022**, *4* (5), 2100279.

(9) Ebbens, S. J.; Gregory, D. A. Catalytic Janus Colloids: Controlling Trajectories of Chemical Microswimmers. *Acc. Chem. Res.* **2018**, *51* (9), 1931−1939.

(10) Kline, T. R.; Paxton, W. F.; Mallouk, T. E.; Sen, A. Catalytic Nanomotors: Remote-Controlled Autonomous Movement of Striped Metallic Nanorods. *Angew. Chem., Int. Ed.* **2005**, *44* (5), 744−746.

(11) Ahmed, S.; Wang, W.; Mair, L. O.; Fraleigh, R. D.; Li, S.; Castro, L. A.; Hoyos, M.; Huang, T. J.; Mallouk, T. E. Steering Acoustically Propelled Nanowire Motors toward Cells in a Biologically Compatible Environment Using Magnetic Fields. *Langmuir* **2013**, *29* (52), 16113−16118.

(12) Ren, L.; Nama, N.; McNeill, J. M.; Soto, F.; Yan, Z.; Liu, W.; Wang, W.; Wang, J.; Mallouk, T. E. 3D Steerable, Acoustically Powered Microswimmers for Single-Particle Manipulation. *Sci. Adv.* **2019**, *5* (10), eaax3084.

(13) Burdick, J.; Laocharoensuk, R.; Wheat, P. M.; Posner, J. D.; Wang, J. Synthetic Nanomotors in Microchannel Networks: Directional Microchip Motion and Controlled Manipulation of Cargo. *J. Am. Chem. Soc.* **2008**, *130* (26), 8164−8165.

(14) Ghosh, A.; Fischer, P. Controlled Propulsion of Artificial Magnetic Nanostructured Propellers. *Nano Lett.* **2009**, *9* (6), 2243−2245.

(15) Dhar, P.; Cao, Y.; Kline, T.; Pal, P.; Swayne, C.; Fischer, T. M.; Miller, B.; Mallouk, T. E.; Sen, A.; Johansen, T. H. Autonomously Moving Local Nanoprobes in Heterogeneous Magnetic Fields. *J. Phys. Chem. C* **2007**, *111* (9), 3607−3613.

(16) Nsamela, A.; Garcia Zintzun, A. I.; Montenegro-Johnson, T. D.; Simmchen, J. Colloidal Active Matter Mimics the Behavior of Biological Microorganisms—An Overview. *Small* **2022**, 2202685.

(17) Peng, F.; Tu, Y.; van Hest, J. C. M.; Wilson, D. A. Self-Guided Supramolecular Cargo-Loaded Nanomotors with Chemotactic Behavior towards Cells. *Angew. Chem.* **2015**, *127* (40), 11828−11831.

(18) Shao, J.; Xuan, M.; Zhang, H.; Lin, X.; Wu, Z.; He, Q. Chemotaxis-Guided Hybrid Neutrophil Micromotors for Targeted Drug Transport. *Angew. Chem., Int. Ed.* **2017**, *56* (42), 12935−12939.

(19) Joseph, A.; Contini, C.; Cecchin, D.; Nyberg, S.; Ruiz-Perez, L.; Gaitzsch, J.; Fullstone, G.; Tian, X.; Azizi, J.; Preston, J.; Volpe, G.; Battaglia, G. Chemotactic Synthetic Vesicles: Design and Applications in Blood-Brain Barrier Crossing. *Sci. Adv.* **2017**, *3*, 13.

(20) Ren, L.; Zhou, D.; Mao, Z.; Xu, P.; Huang, T. J.; Mallouk, T. E. Rheotaxis of Bimetallic Micromotors Driven by Chemical−Acoustic Hybrid Power. *ACS Nano* **2017**, *11* (10), 10591−10598.

(21) Palacci, J.; Sacanna, S.; Abramian, A.; Barral, J.; Hanson, K.; Grosberg, A. Y.; Pine, D. J.; Chaikin, P. M. Artificial Rheotaxis. *Sci. Adv.* **2015**, *1* (4), e1400214.

(22) Katuri, J.; Uspal, W. E.; Simmchen, J.; Miguel-López, A.; Sánchez, S. Cross-Stream Migration of Active Particles. *Sci. Adv.* **2018**, *4* (1), eaao1755.

(23) Li, W.; Wu, X.; Qin, H.; Zhao, Z.; Liu, H. Light-Driven and Light-Guided Microswimmers. *Adv. Funct. Mater.* **2016**, *26* (18), 3164−3171.

(24) Xiao, Z.; Wei, M.; Wang, W. A Review of Micromotors in Confinements: Pores, Channels, Grooves, Steps, Interfaces, Chains, and Swimming in the Bulk. *ACS Appl. Mater. Interfaces* **2019**, *11* (7), 6667−6684.

(25) Simmchen, J.; Katuri, J.; Uspal, W. E.; Popescu, M. N.; Tasinkevych, M.; Sánchez, S. Topographical Pathways Guide Chemical Microswimmers. *Nat. Commun.* **2016**, *7* (1), 10598.

(26) Zhang, L.; Xiao, Z.; Chen, X.; Chen, J.; Wang, W. Confined 1D Propulsion of Metallodielectric Janus Micromotors on Microelectrodes under Alternating Current Electric Fields. *ACS Nano* **2019**, *13* (8), 8842−8853.

(27) McNeill, J.; Sinai, N.; Wang, J.; Oliver, V.; Lauga, E.; Nadal, F.; Mallouk, T. E. Purely Viscous Acoustic Propulsion of Bimetallic Rods. *Phys. Rev. Fluids* **2021**, *6* (9), L092201.
(28) Balk, A. L.; Mair, L. O.; Mathai, P. P.; Patrone, P. N.; Wang, W.; Ahmed, S.; Mallouk, T. E.; Liddle, J. A.; Stavis, S. M. Kilohertz Rotation of Nanorods Propelled by Ultrasound, Traced by Microvortex Advection of Nanoparticles. *ACS Nano* **2014**, *8* (8), 8300−8309.
(29) Zhou, C.; Zhao, L.; Wei, M.; Wang, W. Twists and Turns of Orbiting and Spinning Metallic Microparticles Powered by Megahertz Ultrasound. *ACS Nano* **2017**, *11* (12), 12668−12676.
(30) Wang, W.; Castro, L. A.; Hoyos, M.; Mallouk, T. E. Autonomous Motion of Metallic Microrods Propelled by Ultrasound. *ACS Nano* **2012**, *6* (7), 6122−6132.
(31) Mohanty, S.; Zhang, J.; McNeill, J. M.; Kuenen, T.; Linde, F. P.; Rouwkema, J.; Misra, S. Acoustically-Actuated Bubble-Powered Rotational Micro-Propellers. *Sens. Actuators, B* **2021**, *347*, 130589.
(32) McNeill, J. M.; Nama, N.; Braxton, J. M.; Mallouk, T. E. Wafer-Scale Fabrication of Micro- to Nanoscale Bubble Swimmers and Their Fast Autonomous Propulsion by Ultrasound. *ACS Nano* **2020**, *14* (6), 7520−7528.
(33) Aghakhani, A.; Yasa, O.; Wrede, P.; Sitti, M. Acoustically Powered Surface-Slipping Mobile Microrobots. *Proc. Natl. Acad. Sci. U.S.A.* **2020**, *117* (7), 3469−3477.
(34) Louf, J.-F.; Bertin, N.; Dollet, B.; Stephan, O.; Marmottant, P. Hovering Microswimmers Exhibit Ultrafast Motion to Navigate under Acoustic Forces. *Adv. Mater. Interfaces* **2018**, *5* (16), 1800425.
(35) Bertin, N.; Spelman, T. A.; Stephan, O.; Gredy, L.; Bouriau, M.; Lauga, E.; Marmottant, P. Propulsion of Bubble-Based Acoustic Microswimmers. *Phys. Rev. Applied* **2015**, *4* (6), 064012.
(36) Ahmed, D.; Lu, M.; Nourhani, A.; Lammert, P. E.; Stratton, Z.; Muddana, H. S.; Crespi, V. H.; Huang, T. J. Selectively Manipulable Acoustic-Powered Microswimmers. *Sci. Rep* **2015**, *5* (1), 9744.
(37) Sabrina, S.; Tasinkevych, M.; Ahmed, S.; Brooks, A. M.; Olvera de la Cruz, M.; Mallouk, T. E.; Bishop, K. J. M. Shape-Directed Microspinners Powered by Ultrasound. *ACS Nano* **2018**, *12* (3), 2939−2947.
(38) Sadhal, S. S. Acoustofluidics 15: Streaming with Sound Waves Interacting with Solid Particles. *Lab Chip* **2012**, *12* (15), 2600.
(39) Wiklund, M.; Green, R.; Ohlin, M. Acoustofluidics 14: Applications of Acoustic Streaming in Microfluidic Devices. *Lab Chip* **2012**, *12* (14), 2438.
(40) Raney, W. P.; Corelli, J. C.; Westervelt, P. J. Acoustical Streaming in the Vicinity of a Cylinder. *J. Acoust. Soc. Am.* **1954**, *26* (6), 1006−1014.
(41) Nyborg, W. L. Acoustic Streaming near a Boundary. *J. Acoust. Soc. Am.* **1958**, *30* (4), 329−339.
(42) Tang, Q.; Hu, J. Diversity of Acoustic Streaming in a Rectangular Acoustofluidic Field. *Ultrasonics* **2015**, *58*, 27−34.
(43) Červenka, M.; Bednařík, M. Variety of Acoustic Streaming in 2D Resonant Channels. *Wave Motion* **2016**, *66*, 21−30.
(44) Elder, S. A. Cavitation Microstreaming. *J. Acoust. Soc. Am.* **1959**, *31* (1), 54−64.
(45) Huang, P.-H.; Xie, Y.; Ahmed, D.; Rufo, J.; Nama, N.; Chen, Y.; Chan, C. Y.; Huang, T. J. An Acoustofluidic Micromixer Based on Oscillating Sidewall Sharp-Edges. *Lab Chip* **2013**, *13* (19), 3847.
(46) Zhang, C.; Guo, X.; Royon, L.; Brunet, P. Unveiling of the Mechanisms of Acoustic Streaming Induced by Sharp Edges. *Phys. Rev. E* **2020**, *102* (4), 043110.
(47) Ahmed, D.; Mao, X.; Shi, J.; Juluri, B. K.; Huang, T. J. A Millisecond Micromixer via Single-Bubble-Based Acoustic Streaming. *Lab Chip* **2009**, *9* (18), 2738.
(48) Zhou, M.; Gao, D.; Yang, Z.; Zhou, C.; Tan, Y.; Wang, W.; Jiang, Y. Streaming-Enhanced, Chip-Based Biosensor with Acoustically Active, Biomarker-Functionalized Micropillars: A Case Study of Thrombin Detection. *Talanta* **2021**, *222*, 121480.
(49) Ma, Z.; Zhou, Y.; Cai, F.; Meng, L.; Zheng, H.; Ai, Y. Ultrasonic Microstreaming for Complex-Trajectory Transport and Rotation of Single Particles and Cells. *Lab Chip* **2020**, *20* (16), 2947−2953.
(50) Shen, H.; Zhao, K.; Wang, Z.; Xu, X.; Lu, J.; Liu, W.; Lu, X. Local Acoustic Fields Powered Assembly of Microparticles and Applications. *Micromachines* **2019**, *10* (12), 882.
(51) Lu, X.; Zhao, K.; Peng, H.; Li, H.; Liu, W. Local Enhanced Microstreaming for Controllable High-Speed Acoustic Rotary Microsystems. *Phys. Rev. Applied* **2019**, *11* (4), 044064.
(52) Lu, X.; Martin, A.; Soto, F.; Angsantikul, P.; Li, J.; Chen, C.; Liang, Y.; Hu, J.; Zhang, L.; Wang, J. Parallel Label-Free Isolation of Cancer Cells Using Arrays of Acoustic Microstreaming Traps. *Adv. Mater. Technol.* **2019**, *4* (2), 1800374.
(53) Lu, X.; Soto, F.; Li, J.; Li, T.; Liang, Y.; Wang, J. Topographical Manipulation of Microparticles and Cells with Acoustic Microstreaming. *ACS Appl. Mater. Interfaces* **2017**, *9* (44), 38870−38876.
(54) Behdani, B.; Wang, K.; Silvera Batista, C. A. Electric Polarizability of Metallodielectric Janus Particles in Electrolyte Solutions. *Soft Matter* **2021**, *17* (41), 9410−9419.
(55) Howse, J. R.; Jones, R. A. L.; Ryan, A. J.; Gough, T.; Vafabakhsh, R.; Golestanian, R. Self-Motile Colloidal Particles: From Directed Propulsion to Random Walk. *Phys. Rev. Lett.* **2007**, *99* (4), 048102.
(56) Ebbens, S. J.; Howse, J. R. Direct Observation of the Direction of Motion for Spherical Catalytic Swimmers. *Langmuir* **2011**, *27* (20), 12293−12296.
(57) Mano, T.; Delfau, J.-B.; Iwasawa, J.; Sano, M. Optimal Run-and-Tumble−Based Transportation of a Janus Particle with Active Steering. *Proc. Natl. Acad. Sci. U.S.A.* **2017**, *114*, 13.
(58) Gangwal, S.; Cayre, O. J.; Bazant, M. Z.; Velev, O. D. Induced-Charge Electrophoresis of Metallodielectric Particles. *Phys. Rev. Lett.* **2008**, *100* (5), 058302.
(59) Yan, J.; Han, M.; Zhang, J.; Xu, C.; Luijten, E.; Granick, S. Reconfiguring Active Particles by Electrostatic Imbalance. *Nat. Mater.* **2016**, *15* (10), 1095−1099.
(60) Boymelgreen, A.; Yossifon, G. Observing Electrokinetic Janus Particle−Channel Wall Interaction Using Microparticle Image Velocimetry. *Langmuir* **2015**, *31* (30), 8243−8250.
(61) Campbell, A. I.; Ebbens, S. J.; Illien, P.; Golestanian, R. Experimental Observation of Flow Fields around Active Janus Spheres. *Nat. Commun.* **2019**, *10* (1), 3952.
(62) Katuri, J.; Uspal, W. E.; Popescu, M. N.; Sánchez, S. Inferring Non-Equilibrium Interactions from Tracer Response near Confined Active Janus Particles. *Sci. Adv.* **2021**, *7* (18), eabd0719.
(63) Lyu, X.; Liu, X.; Zhou, C.; Duan, S.; Xu, P.; Dai, J.; Chen, X.; Peng, Y.; Cui, D.; Tang, J.; Ma, X.; Wang, W. Active, Yet Little Mobility: Asymmetric Decomposition of H_2O_2 Is Not Sufficient in Propelling Catalytic Micromotors. *J. Am. Chem. Soc.* **2021**, *143* (31), 12154−12164.
(64) Yang, L.; Chen, X.; Wang, L.; Hu, Z.; Xin, C.; Hippler, M.; Zhu, W.; Hu, Y.; Li, J.; Wang, Y.; Zhang, L.; Wu, D.; Chu, J. Targeted Single-Cell Therapeutics with Magnetic Tubular Micromotor by One-Step Exposure of Structured Femtosecond Optical Vortices. *Adv. Funct. Mater.* **2019**, *29* (45), 1905745.
(65) Boymelgreen, A. M.; Balli, T.; Miloh, T.; Yossifon, G. Active Colloids as Mobile Microelectrodes for Unified Label-Free Selective Cargo Transport. *Nat. Commun.* **2018**, *9* (1), 760.
(66) Demirörs, A. F.; Akan, M. T.; Poloni, E.; Studart, A. R. Active Cargo Transport with Janus Colloidal Shuttles Using Electric and Magnetic Fields. *Soft Matter* **2018**, *14* (23), 4741−4749.
(67) Spatafora-Salazar, A.; Lobmeyer, D. M.; Cunha, L. H. P.; Joshi, K.; Biswal, S. L. Hierarchical Assemblies of Superparamagnetic Colloids in Time-Varying Magnetic Fields. *Soft Matter* **2021**, *17* (5), 1120−1155.
(68) Kim, K.; Guo, J.; Xu, X.; Fan, D. (Emma). Micromotors with Step-Motor Characteristics by Controlled Magnetic Interactions among Assembled Components. *ACS Nano* **2015**, *9* (1), 548−554.
(69) Shen, Z.; Lintuvuori, J. S. Hydrodynamic Clustering and Emergent Phase Separation of Spherical Spinners. *Phys. Rev. Research* **2020**, *2* (1), 013358.

https://doi.org/10.1021/acsnano.2c11070
ACS Nano 2023, 17, 4729−4739

(70) Salari, A.; Appak-Baskoy, S.; Ezzo, M.; Hinz, B.; Kolios, M. C.; Tsai, S. S. H. Dancing with the Cells: Acoustic Microflows Generated by Oscillating Cells. *Small* **2020**, *16* (9), 1903788.
(71) Ahmed, D.; Ozcelik, A.; Bojanala, N.; Nama, N.; Upadhyay, A.; Chen, Y.; Hanna-Rose, W.; Huang, T. J. Rotational Manipulation of Single Cells and Organisms Using Acoustic Waves. *Nat. Commun.* **2016**, *7* (1), 11085.
(72) Kurashina, Y.; Takemura, K.; Friend, J. Cell Agglomeration in the Wells of a 24-Well Plate Using Acoustic Streaming. *Lab Chip* **2017**, *17* (5), 876−886.
(73) Xu, T.; Huang, C.; Lai, Z.; Wu, X. Independent Control Strategy of Multiple Magnetic Flexible Millirobots for Position Control and Path Following. *IEEE Trans. Robot.* **2022**, *38*, 2875.
(74) Khalesi, R.; Nejat Pishkenari, H.; Vossoughi, G. Independent Control of Multiple Magnetic Microrobots: Design, Dynamic Modelling, and Control. *J. Micro-Bio Robot* **2020**, *16* (2), 215−224.
(75) Chowdhury, S.; Jing, W.; Cappelleri, D. Towards Independent Control of Multiple Magnetic Mobile Microrobots. *Micromachines* **2016**, *7* (1), 3.
(76) Tottori, S.; Sugita, N.; Kometani, R.; Ishihara, S.; Mitsuishi, M. Selective Control Method for Multiple Magnetic Helical Microrobots. *J. Micro-Nano Mech.* **2011**, *6* (3−4), 89−95.
(77) Vach, P. J.; Klumpp, S.; Faivre, D. Steering Magnetic Micropropellers along Independent Trajectories. *J. Phys. D: Appl. Phys.* **2016**, *49* (6), 065003.
(78) Bruus, H. Acoustofluidics 7: The Acoustic Radiation Force on Small Particles. *Lab Chip* **2012**, *12* (6), 1014.
(79) Riley, N. Steday Streaming. *Annu. Rev. Fluid Mech.* **2001**, *33* (1), 43−65.
(80) Xu, T.; Soto, F.; Gao, W.; Dong, R.; Garcia-Gradilla, V.; Magaña, E.; Zhang, X.; Wang, J. Reversible Swarming and Separation of Self-Propelled Chemically Powered Nanomotors under Acoustic Fields. *J. Am. Chem. Soc.* **2015**, *137* (6), 2163−2166.
(81) Hoyos, M.; Castro, A. Controlling the Acoustic Streaming by Pulsed Ultrasounds. *Ultrasonics* **2013**, *53* (1), 70−76.
(82) Goia, D.; Matijevic, E. Tailoring the Particle Size of Monodispersed Colloidal Gold. *Colloids Surf., A* **1999**, *146* (1−3), 139−152.
(83) Xu, P.; Duan, S.; Xiao, Z.; Yang, Z.; Wang, W. Light-Powered Active Colloids from Monodisperse and Highly Tunable Microspheres with a Thin TiO_2 Shell. *Soft Matter* **2020**, *16* (26), 6082−6090.
(84) Zhu, J.; Wang, H.; Zhang, Z. Shape-Tunable Janus Micromotors via Surfactant-Induced Dewetting. *Langmuir* **2021**, *37* (16), 4964−4970.

https://doi.org/10.1021/acsnano.2c11070
ACS Nano 2023, 17, 4729−4739